This article can be cited before page numbers have been issued, to do this please use: A. K. Manna, S. Chowdhury and G. K. Patra, *New J. Chem.*, 2020, DOI: 10.1039/D0NJ01954B.

Combined experimental and theoretical studies on Phenyl thiadiazole based novel *turn-on* fluorescent colorimetric Schiff base chemosensor for the selective and sensitive detection of Al³⁺

Amit Kumar Manna,ᵃ Shubhamoy Chowdhuryᵇ and Goutam K. Patraᵃ*

ᵃ**Department of Chemistry, Guru Ghasidas Vishwavidyalaya, Bilaspur (C.G), India**

ᵇ**Department of Chemistry, Gour Banga University, Malda, West Bengal   732 103, India**

Abstract

Herein, we have presented phenyl thiadiazole based Schiff base receptor, 2-[(Z)-(5-phenyl-1,3,4-thiadiazol-2-ylimino)methyl]-6-methoxy-4-nitrophenol (**L**) for the first time for *turn-on* fluorescent, colourimetric detection of Al³⁺ ion. The chemosensor **L** displayed very quick response, excellent selectivity and sensitivity towards Al³⁺ ion in methanol-*tris*-HCl buffer medium (10 mM, pH 7.2, 1:1 v/v) with colourimetric and fluorometric detection limit values 1.43×10^{-7} M and 1.15×10^{-7} M, respectively. The binding stoichiometry was obtained as 2:1 from job's plot analysis and ESI-MS spectra with the association constant value of 1.76×10^{2} M$^{-1/2}$. The experimental results have further been supported by thorough DFT and TD-DFT studies. The chemosensor **L** can be applied for the formation of binary logical devices, recovery of contaminated water samples and smartphone-based chemical analysis.

New Journal of Chemistry Accepted Manuscript

Introduction

In supramolecular chemistry, the analyte sensing by a suitable chemoreceptor primarily depends on host-guest binding through non-covalent interaction like hydrogen bonding, metal-ligand coordination, van der Waals interactions etc.[1-3] Depending on the nature of the emitted signal; it was named as electrochemical, potentiometric and optical sensor.[4] In the case of optical chemosensor, two main processes, like selective recognition and signal transformation, take place during analyte detection. The cavity size, the hardness of the coordinating atom and flexibility of chelator maintain the selectivity by stabilising the host-guest interaction, where as the guest induced electronic/energy change of the chromo/fluorophore produces a proper analytical signal.[5] Upon incorporation of selective analytes not always produce measurable optical signal; thus proper functioning of tailor-made chemosensor is indispensable to generate signal through absorption and/or emission change during host-guest interaction.[6]

Recently the emission-based analyte sensing studies have been performed parallelly with the absorption-based colourimetric measurements, due to its extraordinary sensitivity. Several non-radiative deactivation pathways such as photo-induced electron transfer (PET),[7-8] imine ($>C=N$) isomerisation[9-10] or the combination of the both,[11] can quench the fluorescence intensity of the free receptor. In PET process, receptors containing non-bonding electron pair donors, typically N, O atoms are having HOMO energy in between the HOMO-LUMO energy levels of the excited fluorophore. Thus, electron transfer occurs from the free receptor side to the excited fluorophore, i.e. in excited state redox reaction takes place, which can quench the fluorescence. Also, in the excited state, free imine ($>C=N$) bond behaves almost single bond character; thus non-radiative deactivation occurs due to the inter-conversion in both *cis* and *trans* isomers via free rotation. Specific metal ion binding through N, O donor sites and $>C=N$ moiety, restrict these deactivation processes and thus, emission intensity can be enhanced due to chelation enhancement fluorescence effects (CHEF).[12]

Among the metals, aluminium (Al) is the most abundant metal in the earth crust (8.3%) and mainly presents in its trivalent-ionic form Al^{3+}.[13-15] Due to easy availability, it is extensively used in daily life such as food additives, packing materials, water treatments and for several industrial purposes.[16,17] Generally an average of 3-10 mg/day of this metal is consumed by the human body through drinking water and foods, but it has a negligible physiological role.[18,19] High concentrations of Al^{3+} ion is dangerous for living aquatic species like algae, bacteria, fish and plants[20] and inhibit plants growth.[21] Abnormal intake of Al^{3+} ion can cause several adverse effects such as Parkinson diseases, Alzheimer diseases, amyotrophic lateral sclerosis and so on.[22,23] It also acts as a competitive binder for several essential trace metal ions of similar characteristics like Mg^{2+}, Ca^{2+}

and Fe^{3+} in the body; thus may reduce their activity.[24,25] Accordingly, for human concern WHO has provided guidelines that the maximum tolerable limit of Al^{3+} ions in the body is not more than 10 mg/day.[26]

Some classical analytical techniques like chromatography,[27] inductively coupled plasma emission spectroscopy (ICP-ES),[28] potentiometry[29] and atomic absorption spectroscopy (AAS)[30] were used earlier for the detection of metal ions like Al^{3+}. Due to major drawbacks in terms of troublesome sample preparation, selectivity, sensitivity, time-consuming, and requirement of skilled personnel, chemosensor is used as an alternating method for detection and quantification of Al^{3+}.[31] Recently many optical chemo-receptors have been constructed by some Schiff base host, as the >C=N backbone with proper substituent provided a suitable platform for metal ion sensing in aqueous or semi-aqueous medium.[32] When the Schiff base chemosensor was constructed for selective chelation of Al^{3+} ion, it has great demand because unlike other metal ions, Al^{3+} sensing has lack of spectroscopic characteristics like charge transfer process and formation of insoluble $Al(OH)_3$ due to its high charge density. Thus optical-based chemosensor for precise detection and quantification of Al^{3+} ion is still challenging.

From the above-mentioned facts and in continuation to our current research interest on searching on fluorescent-colourimetric Schiff base chemosensor,[33-35] we have designed and synthesised 5-phenyl-1,3,4-thiadiazole based novel *turn-on* fluorescent, colourimetric Schiff base chemoreceptor **L** by combining one thiadiazole unit with a salicylaldehyde derivative. During the synthesis of chemoreceptor **L**, -OH and -N rich hard basic centre, soft -S moiety along with borderline imine (-C=N) site has been introduced in the skeleton of **L** for interaction with metal ions rapidly. Here, electron-donating methoxy group has been utilised to generate strong ligand field environment and chromophoric nitro group substituted moiety has been selected to visualise colour through extra conjugation. As expected, proposed receptor **L** can properly sense Al^{3+} ion both colourimetrically and *turn-on* fluorometrically in an aqueous medium. The recognition process was further confirmed by the DFT studies, and it has been applied in real sample analysis, smartphone-based analysis and in the building of molecular logic gates.

Experimental

Materials and General information

All the required materials used for synthesis were obtained from Sigma-Aldrich and directly used. The analytical grade solvents used for the overall experiments and freshly prepared double deionised water was used for dilution purpose and preparing *tris* HCl buffer (10 mM, pH=7.2) solution. The metal ion solutions were prepared from their nitrate salts. ^{1}H NMR and ^{13}C NMR

spectra were recorded on a Bruker DRX spectrometer operating at 400MHz in DMSO-d_6 solvent, and chemical shifts were recorded in ppm relative to TMS. Absorption spectra were recorded on a Shimadzu UV 1800 spectrophotometer using 10 mm path length quartz cuvettes with the wavelength in the range of 200-800 nm. High-resolution mass (HRMs) spectra were recorded on a Waters mass spectrometer using mixed solvent HPLC methanol and triple distilled water. The pH measurements were done using a digital pH meter (Merck) by adjusting dilute hydrochloric acid and sodium hydroxide in a buffer solution. Solutions of the receptor **L** (1×10^{-5} M) and metal salts (1×10^{-4} M) were prepared in methanol-*tris*-HCl buffer (10 mM, pH 7.2) medium (1:1 v/v) and H_2O respectively.

X-ray data collection and structural determination

X-ray single-crystal data were collected using MoKα (λ = 0.7107 Å) radiation on a BRUKER APEX II diffractometer equipped with a CCD area detector. Data collection, data reduction, structure solution/refinement were carried out using the software package of SMART APEX.[36] The structures were solved by direct methods (*SHELXS-97*) and standard Fourier techniques, and refined on *F2* using full-matrix least-squares procedures (*SHELXL-97*) using the *SHELX-97* package[37] incorporated in *WinGX*.[38] In most of the cases, non-hydrogen atoms were treated anisotropically. Hydrogen atoms were fixed geometrically at their calculated positions following riding atom model. The crystallographic data of 5-phenyl-1,3,4-thiadiazol-2-amine (**1**), the precursor of **L** has been listed in Table 1. Structural information of **1** has been deposited at the Cambridge Crystallographic Data Center (CCDC number 1993595).

Synthesis of 5-phenyl-1,3,4-thiadiazol-2-amine (1)

5-phenyl-1,3,4-thiadiazol-2-amine (**1**), the precursor of **L**, has been synthesised by following the reported procedure[39] with some modification. Initially, we prepared the individual hot methanolic solution of benzaldehyde, 1.06 gm. (10 mmol) in 15 mL and thiosemicarbazide 0.75 gm. (10 mmol) in 15 mL and then mixed these two solutions. This mixture was refluxed for 2h at 70⁰C. Thiosemicarbazone was obtained as colourless crystal after slow evaporation of methanol which was further used in the next step without purification and characterisation. The thiosemicarbazone and FeCl$_3$ (30 mmol) were dissolved in 15 mL distilled water and heated to 80-90° for 1 hour. A mixture of citric acid (22 mmol) and sodium citrate (10 mmol) were added to the hot solution and again stirred for 2h. After cooling the solution, neutralised with 10% aqueous ammonia. The brown product was filtered out, dried and re-crystallised with methanol. Brown needle-like crystals were obtained on evaporation of methanol solvent, which were suitable for single crystal XRD analysis. Yield, 1.362 g, 77%; mp. >220⁰C. *Anal.* Calc. for $C_8H_7N_3S$: C, 54.22; H, 3.98; N, 23.71. Found C, 54.37; H, 3.93; N, 23.81%. ESI–MS: *m/z* 178.04 (**1**-H$^+$, 100%) (Fig. S1). **^{1}H** NMR (400 MHz,

DMSO-d_6, TMS, J in Hz): δ 7.76-7.74 (2H, NH$_2$, J=6.8), 7.49-7.42 (5H, aromatic protons, J=2; 6.4; 7.6; 11.2) (Fig. S2). ^{13}C NMR (DMSO-d_6, δ ppm, TMS): 168.68, 156.85, 131.43, 130.06, 129.61, 126.77 (Fig. S3).

Synthesis of 2-[(Z)-(5-phenyl-1,3,4-thiadiazol-2-ylimino)methyl]-6-methoxy-4-nitrophenol (L)

0.885 g (5 mmol) of 5-phenyl-1,3,4-thiadiazol-2-amine (**1**) was dissolved in 20 mL of dehydrated methanol and to it 0.985 g (5mmol) of 2-hydroxy-3-methoxy-5-nitrobenzaldehyde (5-nitro *o*- vanillin) was added dropwise with constant stirring. Then the reaction mixture was refluxed for 12h under dry condition. After the reflux is over, the reaction mixture was kept in air for evaporation; while yellow solid separated out. Yield, 1.47g, 83 %; mp.>200^{0}C. *Anal.* Calc. for C$_{16}$H$_{12}$N$_4$O$_4$S : C, 53.93; H, 3.39; N, 15.72. Found C, 53.84; H, 3.46; N, 15.81%. ESI–MS: *m/z* 357.04 (**L**+H$^+$, 100%) (Fig. S4). FTIR/cm^{-1} (KBr): 3430 (-OH) 3160 (-CH), 1606(vs, C=N), 1556 (vs) 1512 (vs, NO$_2$), 1410 (m), 1312 (m), 1332 (s), 1160 (m), 750 (s), 670 (m) (Fig. S5). ^{1}H NMR (400 MHz, DMSO-d_6, TMS, J in Hz): δ 8.11 (1H, J=2.8), 7.92 (1H, J=2.4), 7.75 (2H, J=1.6; 6.4), 7.49-7.43 (m, 5H, aromatic, J=2.0; 8.4; 7.6; 8.0), 3.99 (s, 3H, OMe) (Fig. S6). ^{13}C NMR (DMSO-d_6, δ ppm, TMS): 189.81, 168.98, 157.36, 156.85, 149.66, 139.55, 131.41, 130.07, 129.61, 126.77, 122.00, 116.29, 110.59, 57.23 (Fig. S7).

Preparation of Stock solution for photophysical measurement

Receptor **L** solution was prepared initially at the concentration level of 1 × 10^{-3} M in 10 mL in methanol-*tris* HCl buffer medium (10mM, pH 7.2) solution (1:1 v/v), then diluted to the desired concentration. Also, the stock solutions of guest ions were prepared separately from their nitrate salts (except sulphate salt of Mn^{2+} and Fe^{2+}) at a concentration of 1 x 10^{-3} M in 10 mL double-deionised water and further diluted to their desired concentration. After mixing **L** with each of the metal ions for a few seconds, absorption and fluorescence spectra were obtained at room temperature.

Computational details

The GAUSSIAN-09 Revision C.01 program package was used for all calculations.[40] The gas-phase geometries of the molecule **L** and its Al^{3+} complex (2**L**+Al^{3+}) were optimised entirely unrestricted of symmetry in singlet ground states with B3LYP functional[41] and LanL2DZ[42] respectively as the basis set. The electronic spectra of the molecule **L** and 2**L**+Al^{3+} were calculated with the TD-DFT method, and the solvent effect (in methanol) was simulated using the polarising continuum model with the integral equation formalism (C-PCM).[43,44] The light-induced electron transfer (LIET) calculation method is a superior to investigate the MLCT/LLCT transitions.[45]

Table 1 Crystal data and structure refinement for **1**.

|	
CCDC Number	1993595
Empirical formula	$C_8H_7N_3S$
Formula weight	177.23
Temperature/K	109.38
Crystal system	monoclinic
Space group	$P2_1/c$
a/Å	11.1251(14)
b/Å	7.5242(7)
c/Å	11.1940(12)
α/°	90
β/°	115.098(15)
γ/°	90
Volume/Å³	848.55(19)
Z	4
ρ_{calc} g/cm³	1.3872
μ/mm⁻¹	0.324
F(000)	368.6
Crystal size/mm³	0.18x0.12x0.10
Radiation	Mo Kα (λ = 0.71073)
2Θ range for data collection/°	4.04 to 52.72
Index ranges	-14 ≤ h ≤ 14, -8 ≤ k ≤ 10, -15 ≤ l ≤ 13
Reflections collected	4133
Independent reflections	1730 [R_{int} = 0.0188, R_{sigma} = 0.0304]
Data/restraints/parameters	1730/0/110
Goodness-of-fit on F^2	1.002
Final R indexes [I>=2σ (I)]	R_1 = 0.0385, wR_2 = 0.0982
Final R indexes [all data]	R_1 = 0.0548, wR_2 = 0.1084
Largest diff. peak/hole / e Å⁻³	0.32/-0.28

Results and discussion

Synthesis and structure of L

Among the most of the N, O based Schiff base receptor for Al^{3+} ion, the proposed chemosensor **L** has been synthesised through the easy and economical procedure with high yield (over 80%) by 1:1 condensation reaction of 5-phenyl-1,3,4-thiadiazol-2-amine (1) and 5-Nitro-o-vanillin (Scheme 1). **1**, the precursor of **L** has also been synthesised by $FeCl_3$ induced cyclisation of thiosemicarbazone (Scheme 1) and its structure was determined by X-ray crystallography. **1** crystallised as monoclinic $P2_1/c$ space group. The ORTEP diagram of **1** has been shown in Fig. S8. In **1**, the bond lengths and angles are in the expected ranges (Table S1 and S2). Unfortunately, we didn't obtain and good-

quality single crystal for **L**. The structure of **L** has been fully characterised by FTIR, ^{1}H-NMR, ^{13}C-NMR, ESI-mass spectra and elemental analyses.
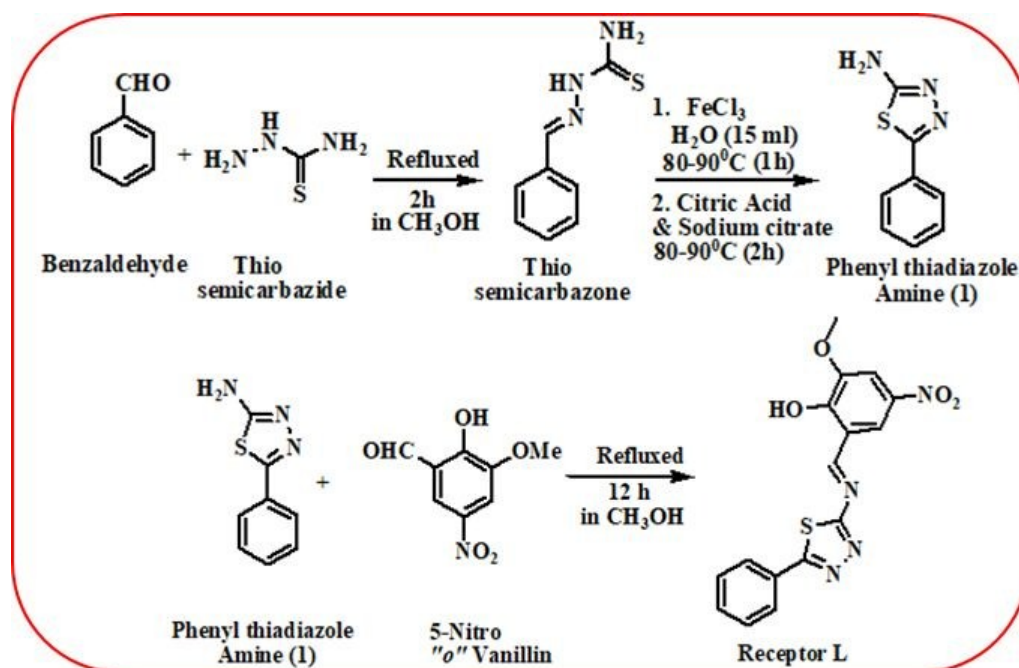
Scheme 1. The synthetic procedure of the probe **L**.

Generally, bioaccumulation of metal ions was mainly originated through water contamination; thus, the organic receptor should be highly water-soluble and can detect analytes in an aqueous medium. Here, the probe **L** cannot be completely soluble in pure water due to the presence of hydrophobic aromatic side-chain; thus, methanol can be used to improve water solubility. Although it is frequently soluble in 1:4 methanol-water binary mixture, the stock solution of **L** has been prepared in methanol-*tris*-HCl buffer medium (10 mM, pH 7.2) solution (1:1 v/v), owing to the stability over 5 days.

UV-Vis Spectroscopic studies of L towards different metal ions

The receptor **L** contains suitable positioned donor–π conjugation-accepter moiety; thus responsible for typical intramolecular charge transfer (ICT), which can influence the photophysical behaviour. In order to check the ICT process, absorption spectra of **L** were taken in the different solvent of variable polarity like dimethylsulfoxide (DMSO), acetonitrile, methanol and chloroform, as the solvent dipole can relax the ICT absorption band[46] through polarisation/ interaction with multiple chromophoric systems. As shown in Table 2, small red-shifted absorption bands of **L** obtained in relatively more polar solvent DMSO in comparison to moderately polar solvent CH_3CN, CH_3OH (Fig. S9) and less polar $CHCl_3$. However, moderately polar solvent MeOH has been selected for further studies, as it is an environmentally benign solvent, well water miscibility and easy to handle.

Table 2 UV-Vis data of **L** in different solvent.

| Solvent	λ_{max}**L**	Logε
Methanol	412 nm	3.58
CH$_3$CN	441 nm	3.50
DMSO	453 nm	3.79
CHCl$_3$	340 nm	4.05

Initially, the metal selective response of the proposed chemosensor **L** has been carried out through UV-Vis spectral studies at room temperature in methanol-*tris*-HCl buffer (10 mM, pH 7.2) solution (1:1 v/v). The absorption maxima of free receptor displayed at 304, 362 and 412 nm corresponding to the existence of two different chromophoric subunits and overall ICT band, which imparts its deep yellow colourisation. Upon monitoring the 2 equivalent of some biologically important metal ions like Na$^+$, K$^+$, Mg^{2+}, Fe^{3+}, Ag$^+$, Cu^{2+}, Mn^{2+}, Co^{2+}, Ni^{2+}, Mn^{7+}, Cr^{6+}, Mo^{6+} and Ga^{3+} to the probe solution, negligible change in absorption spectra was observed, while in the presence of Zn^{2+}, Cd^{2+}, Hg^{2+}, Pb^{2+}, Fe^{2+} and Pd^{2+} the absorption band at 372 nm was enhanced with a decrease at 301 nm due to interaction with S atom of the heterocyclic ring. Unlikely, the addition of only Al^{3+} the absorption band at 412 and 362 nm completely vanished, whereas for Cr^{3+} these bands exist partially. Consistently, the deep yellow colour of receptor solution immediately changed to colourless in case of Al^{3+} ion, very pale yellow in case of Cr^{3+} and intense yellow colour in case of the thiophilic metal ions (Fig. 1a).
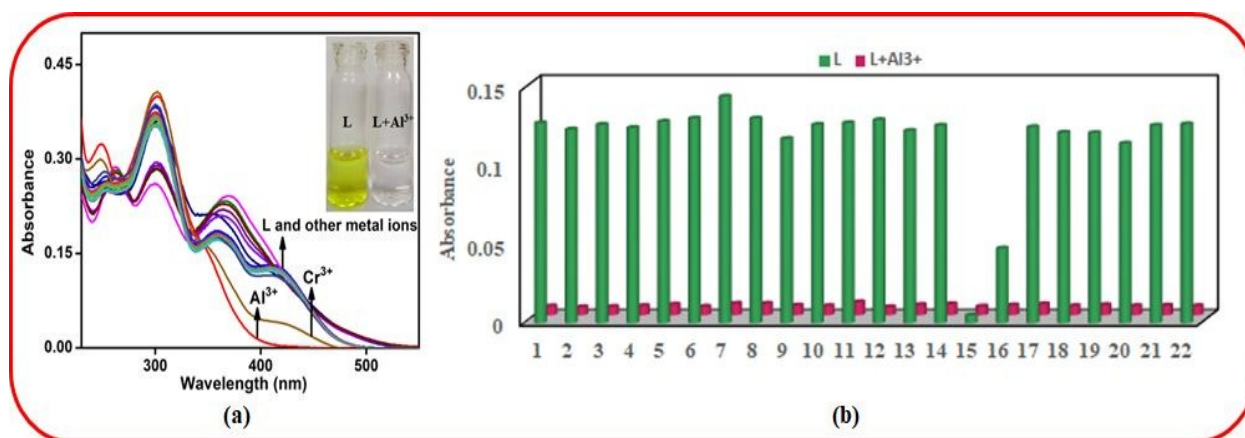
Fig. 1. (a) Absorption spectra of **L** (40 μM) changes in presence of 2 equiv. of different metal ions in methanol-*tris*-HCl buffer (10 mM, pH 7.2) solution (1:1 v/v). Inset: corresponding colour change of the solution; (b) Competitive experiment in presence of **L** and other metal ions (where 1 = **L**, 2 = Na$^+$, 3 = K$^+$, 4 = Mg^{2+}, 5 = Fe^{3+}, 6 = Ni^{2+}, 7 = Co^{2+}, 8 = Cd^{2+}, 9 = Hg^{2+}, 10 = Pb^{2+}, 11 = Cu^{2+}, 12 = Ag$^+$, 13 = Zn^{2+}, 14 = Mn^{2+} 15 = Al^{3+},16 = Cr^{3+}, 17=Mn^{7+}, 18=Cr^{6+}, 19=Mo^{6+}, 20 =Ga^{3+}, 21=Fe^{2+} and 22= Pd^{2+}) in methanol-*tris*-HCl buffer (10 mM, pH 7.2) solution (1:1 v/v).

Achievement of specific Al^{3+} ion selectivity of **L** over other interfering ions is an important feature to construct a chemosensor. Thus the competitive studies were performed in methanol-*tris*-HCl buffer (10 mM, pH 7.2) medium (1:1 v/v) by titrating with all the metal ions systematically into a fixed **L**-Al^{3+} solution. From fig. 1b, Al^{3+} ion can influence the same absorption change of **L**, irrespective the other metal ions present or not. Even in the presence of 5 fold higher concentrations of above-mentioned competitive ions than Al^{3+} ion, the optical behaviour of **L**-Al^{3+} complex remains consistent.

As the receptor **L** contains acid-base sensitive groups like –OH, -OMe and >C=N, the pH range on the sensing process has primarily set through absorption measurements. For this purpose, the ligand solutions were suitably adjusted within pH value ranging from 3 to 12 in a series maintaining identical concentration using 0.1 M HCl and NaOH solution and then absorption studies were performed in the presence of Al^{3+} ion (Fig. 2a). At low pH, multiple coordination sites were protonated, which can retard Al^{3+} binding as well as ICT process. At pH above 10, ICT effect becomes much more predominant in case of **L**, and there was a chance of insoluble $Al(OH)_3$ formation, which can create hindrance for binding. Combining these two effects, the absorption intensity around 412 nm of **L**+Al^{3+} somewhat increases at a highly basic medium. Based on these observations, the sensing studies were performed at pH 7.2 using *tris*-HCl buffer, where the acid-base sensitive groups cannot be disturbed.
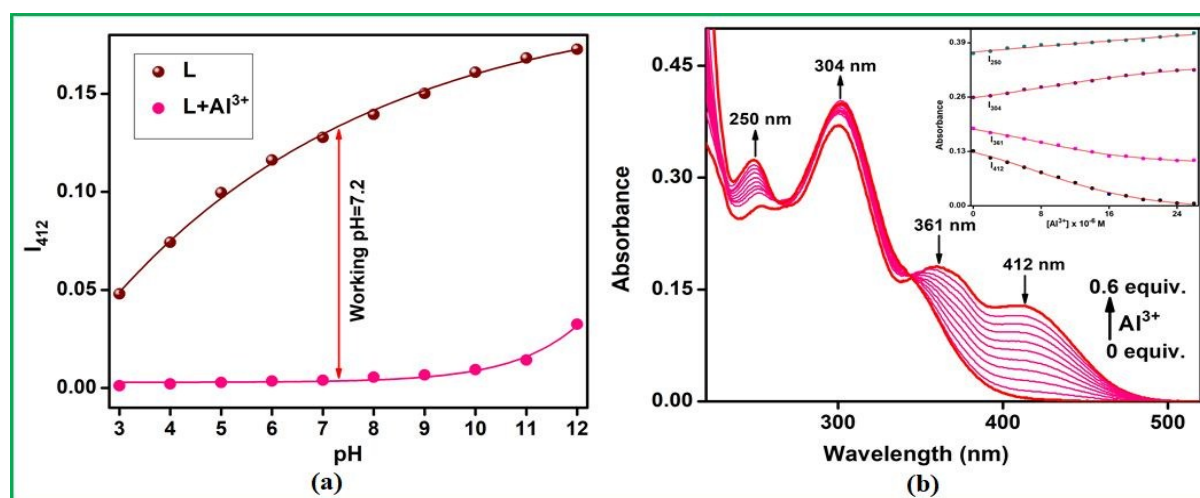

Fig. 2. (a) pH effect of **L** and **L**–Al^{3+}complex (b) absorption titration of **L** with Al^{3+} ion in methanol-*tris*-HCl buffer (10 mM, pH 7.2) solution (1:1 v/v).

In order to get the sensitive response on absorption behaviour of receptor **L** in the presence of Al^{3+} ion binding, titration experiment was conducted in methanol-*tris*-HCl buffer (1:1 v/v, 10 mM, pH 7.2) solution. With the increase in Al^{3+} ion concentration in the ligand **L** solution, both the absorption bands at 361 and 412 nm decreased gradually with a little enhancement of absorption

band 301 and at 250 nm (Fig. 2b). Almost 0.6 equivalent of Al^{3+} ion was enough to reach the saturation of absorption change and the deep yellow colour of the ligand solution transformed to colourless. A well-defined isosbestic point was developed at 345 nm, indicating that both the **L** and **L**+Al^{3+} complex are in dynamical equilibrium. The absorption study and visual colour change primarily indicate that restriction of ICT process of "nitro *ortho*-vanillin" moiety upon Al^{3+} ion complexation, mainly responsible for colourimetric sensing (Scheme 2, *vide infra*). In the free receptor **L**, the -OH group (ICT donor) present in suitable positioned with electron-withdrawing -NO_2 moiety (ICT acceptor) thus intra-molecular charge transfer (ICT) operate in the ground state which imparts the absorption band at 412 nm with yellow colourisation. When the Al^{3+} ion binds with the imine site and the -OH group, the ICT becomes restricted, which decrease in the absorption band at 412 nm and thus, the yellow colour of the medium changed to colourless.

From the titration data, the variation of absorption intensity at 412, 361, 304 and 250 nm with the concentration of Al^{3+} ion has been shown in the inset of fig. 2b. Among these plots, the absorption band at   412 nm, changes much more rapidly with a linear relationship up to 18 μM. The limit of detection (LOD) value was calculated at S/N= 3 to 1.43×10^{-7} M from the linear fitting of this calibration curve based on the convenient formula 3σ/m. From the calibration curve I_{412} *vs.* [Al^{3+}] the slope 'm' and from the absorbance *vs.* [**L**] plot, the standard deviation 'σ' was obtained. The calculated value of LOD, is much lower than the threshold value specified by WHO and many of the previously reported Al^{3+} ion sensors (Fig. 3a).
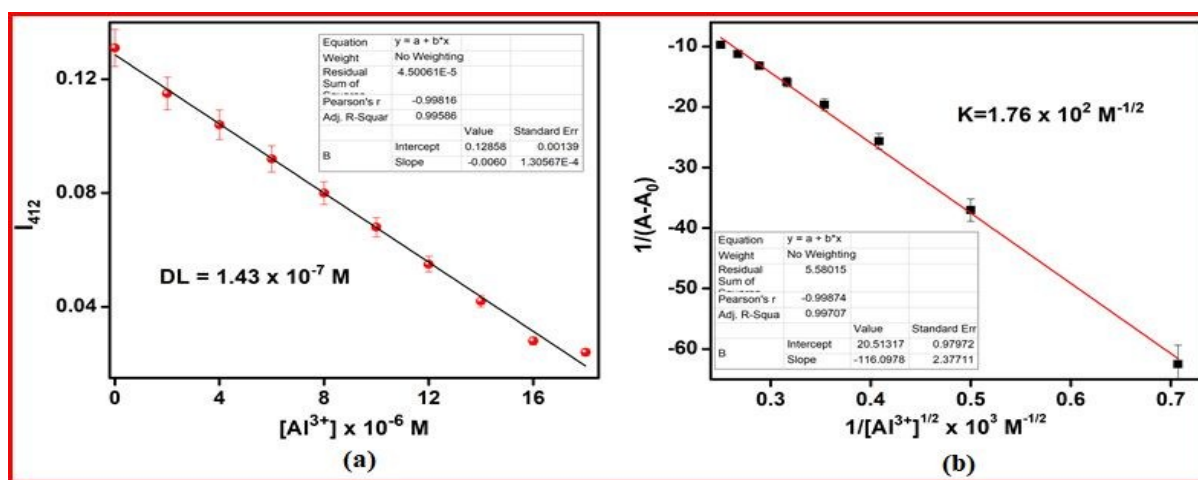

Fig. 3. (a) Colourimetric detection limit of **L** for Al^{3+} and (b) determination of association constant.

To evaluate the binding stoichiometry, the conventional Jobs continuous method analysis was used (Fig. S10). It indicates that the receptor **L** binds with analyte Al^{3+} ion in a 2:1 fashion which was primarily assumed from absorption titration and further confirmed by mass

spectrometry. In the ESI-MS the base peak obtained at m/z = 773.06 corresponds to $2L+Al^{3+}+2H_2O$ (Fig. S11). Assuming 2:1 binding interaction, the association constant value for $L-Al^{3+}$ complex was obtained to 1.76×10^2 $M^{-1/2}$ (Fig. 3b) by the Benesi-Hildebrand (B-H) linear fitting of the inverse of absorption change *vs.* square root of inverse Al^{3+} ion concentration which is highly comparable with the previously reported $2L+Al^{3+}$ complexes.[47]

In order to understand the nature of the binding interaction and re-usability of the present chemosensor **L**, chemical reversibility was verified by absorption spectra in the presence of 1 equiv. of Na_2EDTA in methanol-*tris*-HCl buffer (10 mM, pH 7.2) solution (1:1 v/v). Here the absorption band at 412 and 361 nm immediately appeared on addition of Na_2EDTA to $L-Al^{3+}$ adduct due to the generation of free receptor **L** with a colour change from colourless to yellow. Further addition of excessive Al^{3+} ion, these optical changes almost restored. This alternative conversion of the complexation and de-complexation was almost consistent over 5 cycles with systematic addition of Al^{3+} and Na_2EDTA with negligible loss of absorption intensity (Fig. 4a). Thus the chemosensor **L** is reversible and the acidic Al^{3+} ion binds through chelation rather than any acid catalyst hydrolysis or irreversible reaction.
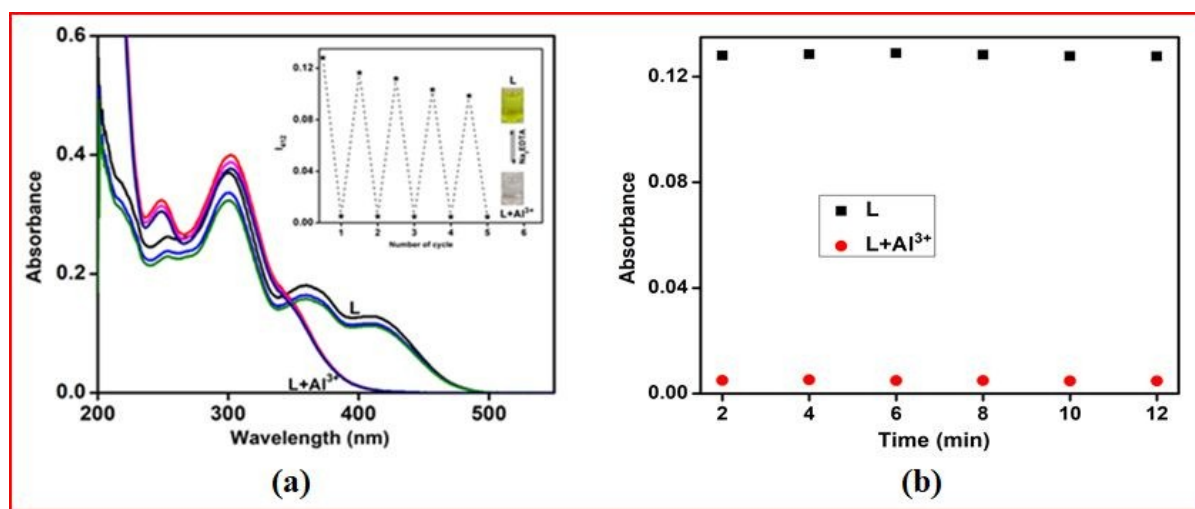

Fig. 4. (a) Reversibility study of **L** with Al^{3+} and Na_2EDTA in methanol-*tris*-HCl buffer (10 mM, pH 7.2) solution (1:1 v/v) (b) Time effect of **L** with Al^{3+} ion detection in methanol-*tris*-HCl buffer (10 mM, pH 7.2) solution (1:1 v/v) by absorption studies.

The time evolution of the receptor **L** for colorimetric Al^{3+} ion sensing was also investigated through absorption spectral measurements in methanol-*tris*-HCl buffer (10 mM, pH 7.2) solution (1:1 v/v) (Fig. 4b). As soon as Al^{3+} ion was added into the receptor solution, the absorption band at 412 nm and 362 nm immediately disappeared with a very quick colour change from colourless to yellow was observed in naked eyes. This colour and absorption changes remain consistent over an

extended period of time. This indicates that the recognition behaviour gets almost completed within 2 minutes and cannot be disturbed up to 12 min, thus can be utilised for monitoring Al^{3+} ion for practical purposes.

Fluorescence studies

The selective emissive properties of the chemosensor **L** towards metal ions, fluorescence measurements were conducted under identical working media in methanol-*tris*-HCl buffer (1:1 v/v, 10 mM, pH 7.2) solution. In free receptor **L**, excitation of phenyl-thiadiazole fluorophore at 310 nm, the moderate emission band at 380 nm was observed. Sequential addition of 2 equiv. of each of the selected metal ions like Na^+, K^+, Mg^{2+}, Zn^{2+}, Cd^{2+}, Hg^{2+}, Pb^{2+}, Fe^{2+}, Pd^{2+}, Al^{3+}, Fe^{3+}, Ag^+, Cu^{2+}, Mn^{2+}, Co^{2+}, Ni^{2+}, Mn^{7+}, Cr^{3+}, Cr^{6+}, Mo^{6+} and Ga^{3+} to the chemosensor **L**, only Al^{3+} ion can enhance the emission intensity much more prominently, whereas the heavy metal ions such as Cd^{2+}, Hg^{2+}, Pb^{2+}, Cu^{2+}, Ag^+ , Zn^{2+}, Pd^{2+} etc. quenched the original emission band of **L** (Fig. 5a). As in the fluorescence quenching process, it is very difficult to differentiate the low-intensity signal from the false pulsing response by the background environment or due to precipitation of the receptor; thus, it is considered that the fluorometric response of the receptor **L** obtained only in the presence of Al^{3+} ion. In the competitive experiments, the Al^{3+} ion depending emission spectra of **L** cannot be disturbed by the presence of other quenching metal ions in equal concentration. Although the 5 fold higher concentration of interfering ions compare to Al^{3+} ion, slightly decrease the intensity but the existence of Al^{3+} ion was still measurable from emission spectra in the mixed solution (Fig. S12).
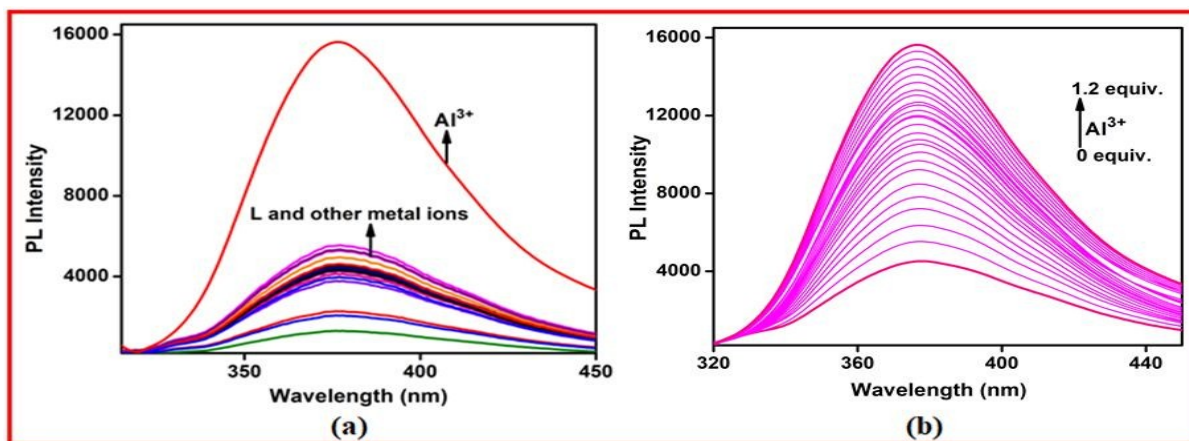
Fig. 5. (a) Fluorescence spectra of **L** in presence of 2 equiv. different metal ions in methanol-*tris*-HCl buffer (10 mM, pH 7.2) solution (1:1 v/v). (b) Fluorescence titration of **L** with Al^{3+} in methanol-*tris*-HCl buffer (10 mM, pH 7.2) solution (1:1 v/v).

The excitation and the emission spectra of **L**, as well as **L**+Al^{3+} have been measured in methanol-*tris*-HCl buffer (10 mM, pH 7.2) solution (1:1 v/v) and shown in Fig. S13. Upon excitation at 310 nm, the free receptor **L** showed moderate emission centred at 380 nm due to some

radiative decay from the excited fluorophore phenyl-thiadiazole. In the chromophore **L**, the PET operates from the –OH site to the excited fluorophore, but its efficiency is very less, as it also participates in delocalisation at the same time with the –NO_2 group. After PET, the single electron in the excited fluorophore comes to the singly vacant orbital of the receptor through back electron transfer (BET) process. In the presence of Al^{3+} ion, the receptor **L** forms a tight complex, which diminished both the PET and >C=N isomerisation processes, and emission intensity is enhanced due to CHEF. In the titration experiments, when the concentration of Al^{3+} ion was increased to the fixed solution of **L**, emission intensity at 380 nm increased gradually and became saturated when the concentration of Al^{3+} reached to 1.2 equiv. (Fig. 5b). In the presence of Al^{3+} ion, the receptor **L** forms a tight complex which diminished both the PET and >C=N isomerisation processes, and emission intensity is enhanced due to CHEF. Furthermore, the emission intensity change showed a linear relationship with the Al^{3+} ion concentration and the detection limit was calculated to 1.15 x 10^{-7} M from this calibration curve using the same formula 3σ/m (Fig. S14). This value is slightly differing from the DL obtained in absorption spectra as the difference in sensitivity of both this spectrophotometer.

Jobs plot analysis has also been performed through fluorometric measurement. 2:1 mode of binding of **L** with the analyte Al^{3+} ion is also confirmed by this measurement (Fig. S15). In pH studies, the emission intensity of host-guest complex is maximum within pH 6.0-9.0 (Fig. 16). Below pH 5.0, H^+ ion is a competitor for Al^{3+} ion binding and above pH 9, there is a chance of insoluble $Al(OH)_3$ formation. Here also the host-guest complex shows reversible behaviour in presence of Na_2EDTA and retained up to three cycles with negligible loss in fluorescence intensity (Fig. S17). In the time evolution of the receptor L in presence of 2 equiv. Al^{3+} ion was also investigated in methanol-*tris*-HCl buffer (10 mM, pH 7.2) solution (1:1 v/v). The strong emission band of **L** at 380 nm due to Al^{3+} recognition, was appeared within 2 min and remains almost unchanged up to 12 min (Fig. 18) emission. This quick fluorometric response time of the receptor **L** towards Al^{3+} ion is very crucial to be a sensitive sensor and can be applied in environmental analysis.

DFT studies on L and 2L-Al^{3+} complex (2)

The optimised structure of **L** and **2** are shown in Fig. 6, and listed their calculated bond distances and angles in Table S1. The bond lengths C1-N1 and C7-O1 of the optimised structure of **L** are 1.305 and 1.367 Å, respectively. The calculated bond length of Al1-N1 in **2** is 2.125 Å and found in the typical range 1.921 to 2.191.[48] The Al1-O1 bond length 1.860 Å of coordinated phenolic oxygen for the optimised structure of **2** is observed in the typical range 1.857-1.885 Å.[49] The bite angle of N1-Al1-O1 is 88.38º for the species **2** falls in the typical range.[50] There is good agreement

between the calculated geometry of the probable structure of **2** species with other reported similar structural data in literature.[48-50]
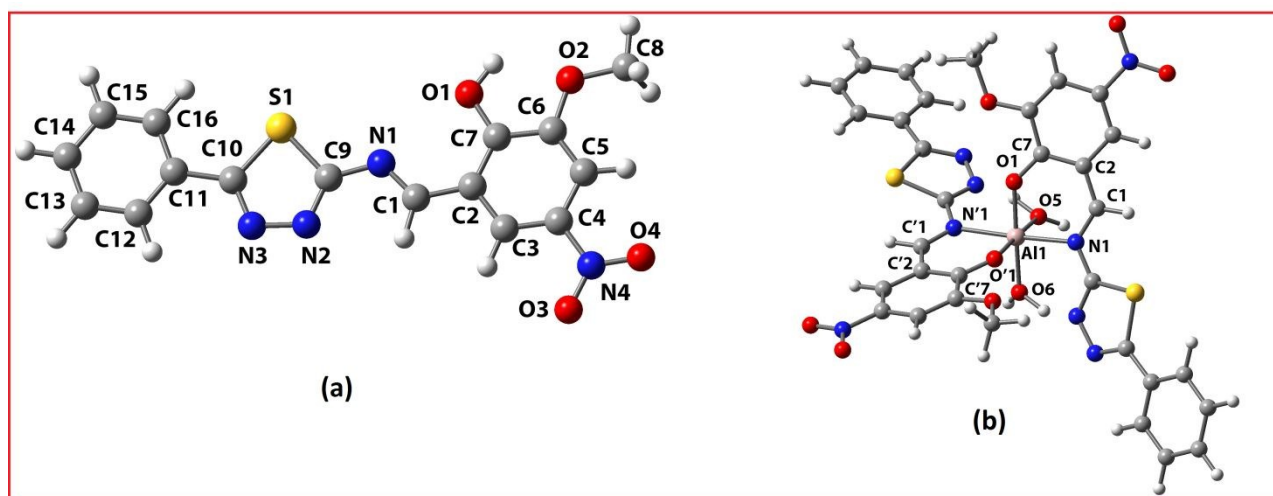

Fig. 6. DFT optimized structures of (a) **L** and (b) 2L-Al^{3+} **(2)**.

Molecular orbital description and Electronic spectra

The absorption spectra of **L** and **2** are simulated in the presence of the solvent model (methanol) employing the TD-DFT methods with the identical basis set and functional as used in geometry optimisation calculations. The spin-allowed electronic transitions are in good harmony with our experimental data (Fig. 7). Calculated spin-allowed singlet-singlet electronic transitions with the experimentally observed data for **L** and **2** in water are summarised in Table S2. The selected transitions of **L** and **2** having significant oscillator strengths are incorporated and also screen the transitions only with orbital contributions larger than 5% are taken into account for molecular ions. A schematic representation of the energy of MOs and contours of selected HOMO and LUMO orbitals of **L** and **2** are presented in Figs S19 and 8. The HOMO to LUMO energy gap for **L** and **2** are 3.380 and 2.881 eV, respectively. The energy transition was calculated at 408.92, and 369.03 nm for **L** and the transition can be assigned as n-n* and/or n-π*. On the basis of molecular orbital analysis, other calculated transition of **L** can be assigned intra ligand charge transfer transitions. In contrary, the calculated transition (H-1→L+1, H-4→L+1) at 377.94 nm for **2** is assigned as metal to ligand charge transfer (MLCT) along with some contribution of ligand to ligand charge transfer (LLCT) and rest of the transitions are assigned as intra ligand charge transfer as well as ligand to π orbitals of coordinated H_2O molecules transitions. The HOMO levels H to H-1 of **2** have partially metallic character. Thus the calculated transitions are either of metal to ligand charge transfer (MLCT) or intra ligand charge transfer transitions and ligand to π orbitals of coordinated H_2O transitions. The above-calculated bands for **L** and **2** are good agreement with the experimentally measured bands in methanol solution and listed in Table S2.
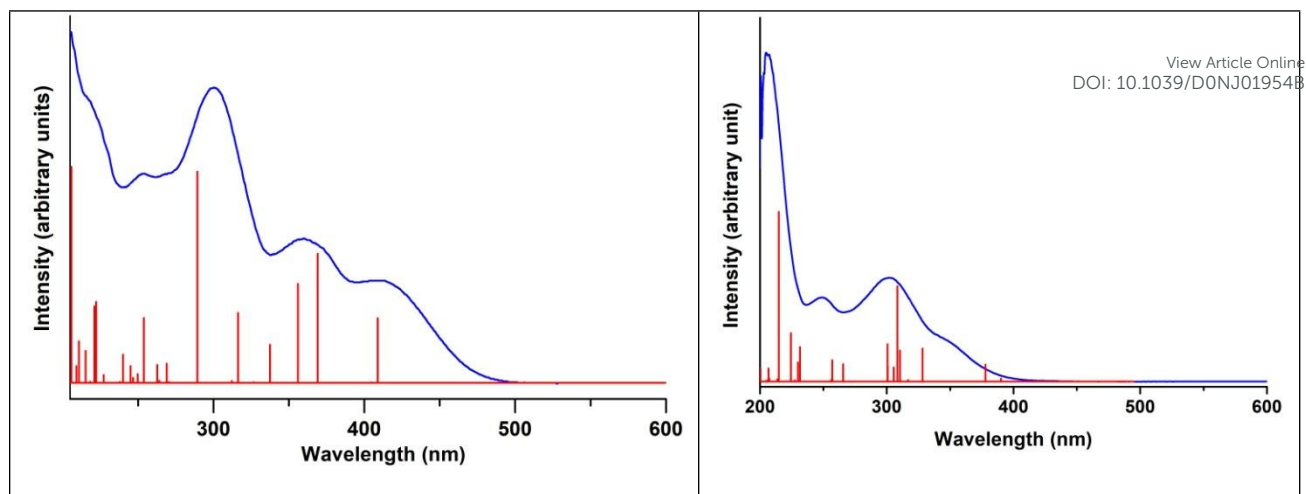
Fig. 7. The experimental (blue) and the calculated electronic transition (red) of **L** (left) and **2** (right).
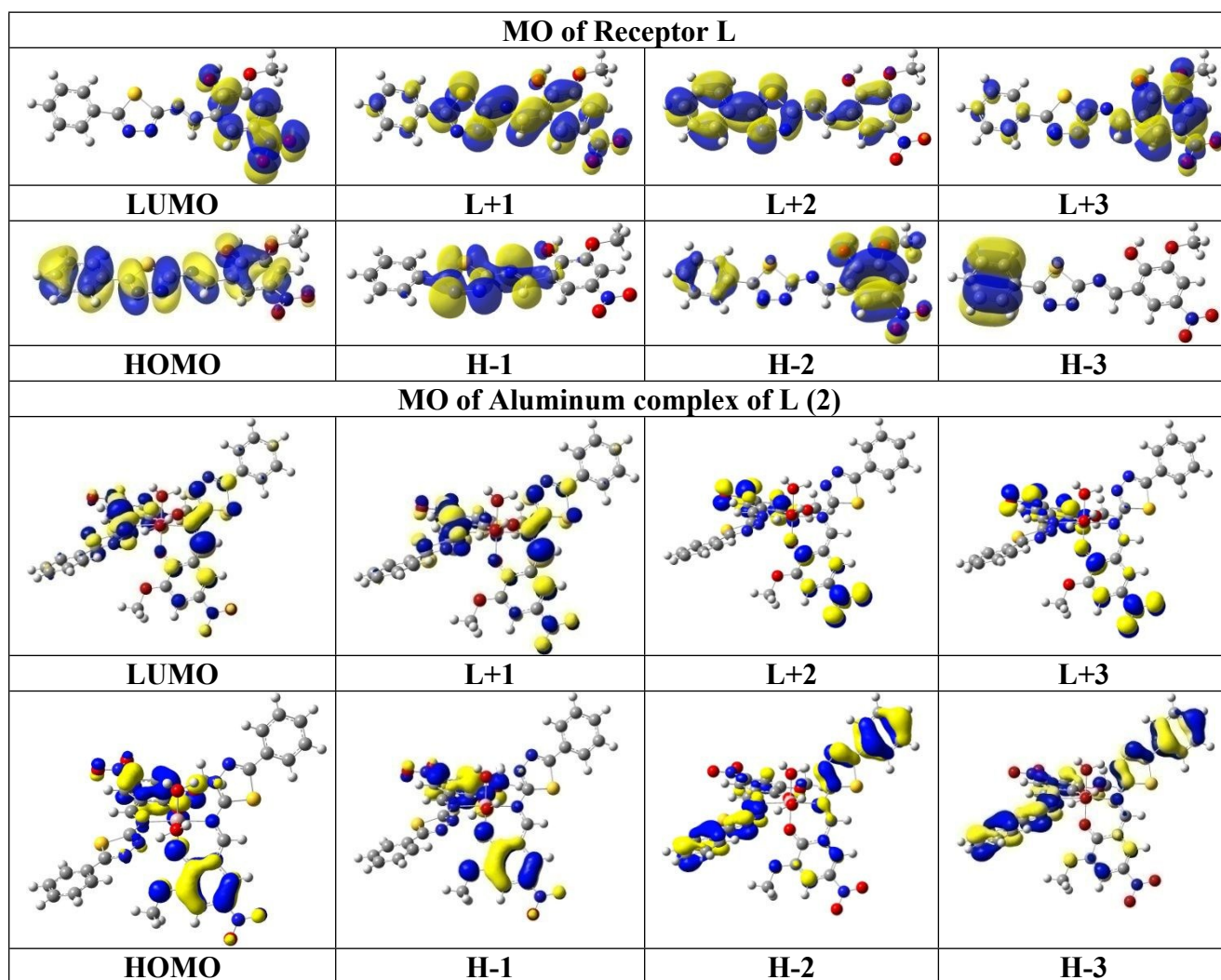
Fig. 8. Selected HOMOs and LUMOs of **L** and **2** are shown. Positive values of the orbital contour are represented in yellow (0.03 au) and negative values in blue (−0.03 au).

Explanation of fluorescence properties from DFT

The probe **L** exhibits a simple approach for the selective detection of Al^{3+} with the enhancement of fluorescence intensity because of the CHEF (chelation-enhanced fluorescence) process after interaction with Al^{3+}. The energy gap between the highest occupied molecular orbital (HOMO) and lowest unoccupied molecular orbital (LUMO) of **L** and **2** are 3.380 and 2.881 eV, respectively. The complex **2** compared to the probe **L** are established with the easy electronic transition and get the additional stability of **2** (Fig. 9). The contours of the electronic distribution in HOMO and LUMO states of these molecules suggested significant energy difference 0.499 eV between **L** and **2**. Specifically, LUMO states of **2** in comparison to **L** revealed that the electrons are more delocalised insight into **2** molecule than the receptor **L** in agreement with the barrier of the photo-induced electron transfer process, which may results in the enhancement of fluorescence through CHEF.[51]
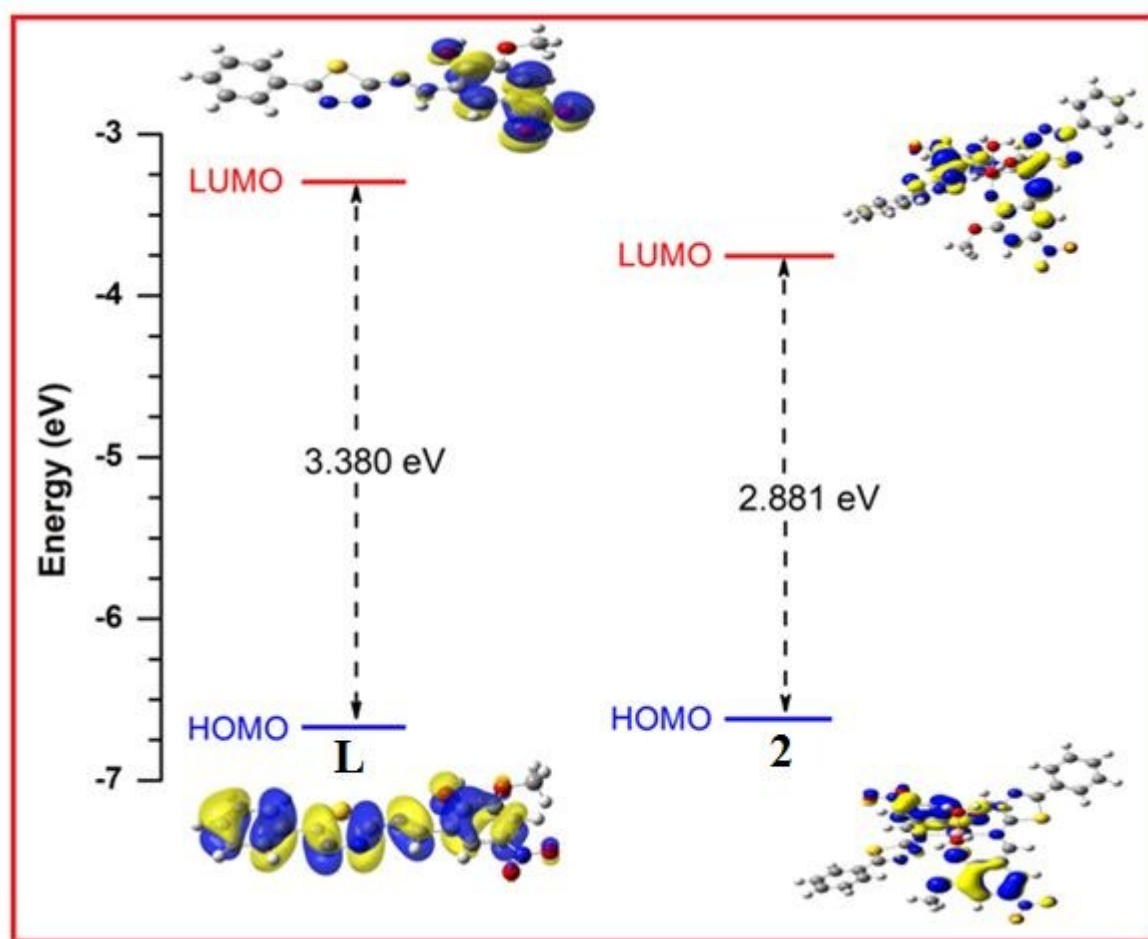

Fig. 9. HOMO-LUMO energy levels of **L** and **2**.

Sensing mechanism

In order to get the actual host-guest structure, we have tried to isolate Al^{3+} complex of **L**, in the form of single crystal but failed. Thus the Al^{3+} binding sites of the receptor **L** were confirmed by FT-IR spectra of the host-guest complex. The initial broad band at 3430 cm^{-1} due to -OH stretching almost vanished in the **L**-Al^{3+} complex (**2**), along with a small vibrational band appeared around at 632 cm^{-1} probably due to Al-O stretching. Also non-existence of vibrational band around 545 to 560 cm^{-1} in **2** indicated that the heterocyclic thiadiazole "N" cannot participate in Al^{3+} ion binding (Fig. S20). The DFT and TDDFT studies of **2**, starring from were also investigated to establish the mechanism and the binding sites (*vide supra*).

Based on the above observations, the detection of the analyte can be explained by the selective Al^{3+} ion capturing and the optical signal change. The receptor **L** contains electron-rich N and O centre, which showed strong affinity towards hard metal like Al^{3+}. The phenolic -OH of the free receptor **L** participate ICT with chromophoric NO_2, which imparts yellow coloured solution in ground state. Also, the reduction of electron density on -O atom, extends PET from phenolic -OH to phenyl-thiadiazole fluorophore, is also weak, and the receptor **L** showed moderate emission. After the Al^{3+} ion binding through O and imine site, the colour changes from yellow to colourless due to restriction of ICT and emission enhancement through CHEF due to retardation of both PET and imine isomerisation. Here the two heterocyclic N atoms of the probe **L** cannot participate in actual analyte binding but can preferably select the small Al^{3+} ion to sit inside the cavity. Thus from the absorption and emission titration, Job's plot, FT-IR, ESI-MS spectra, and DFT-TDDFT studies the plausible sensing mechanism has been established (Scheme 2).
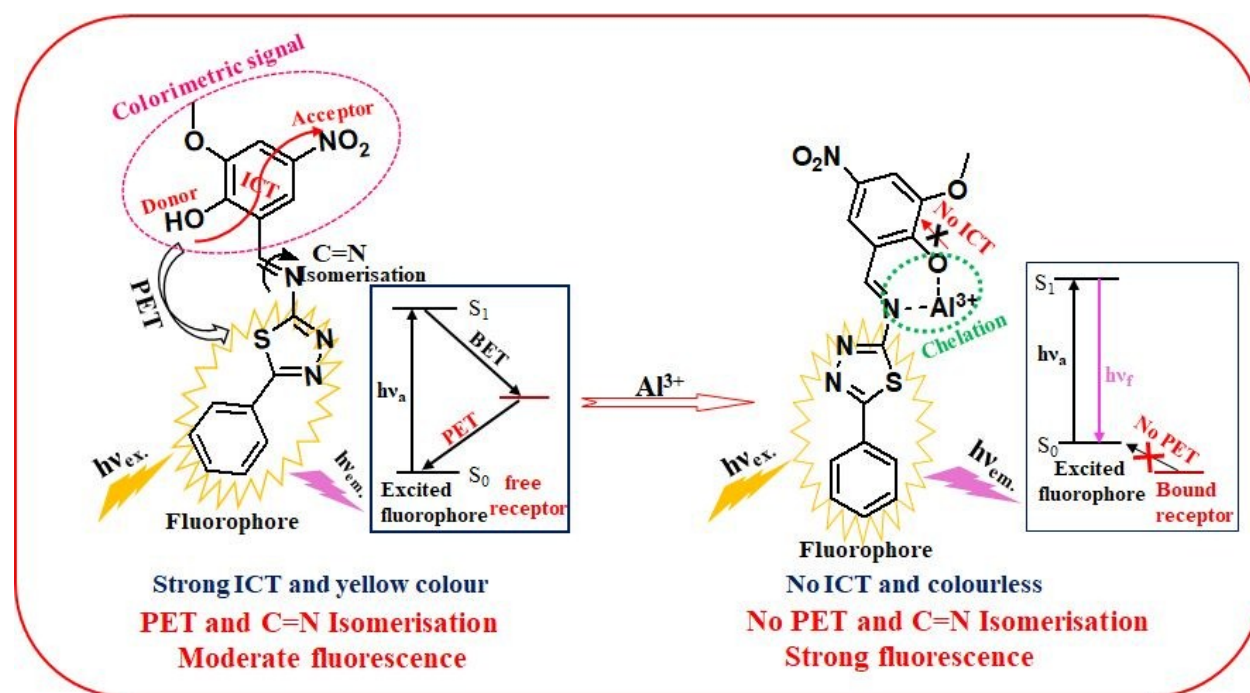
Scheme 2. Plausible sensing mechanism.

Application of chemosensor L in real samples

To explore the Al^{3+} sensing ability of the present chemosensor **L** in real water samples, we have initially tested with laboratory tap water samples by colorimetric and fluorometric methods. The Al^{3+} ion concentration of the tap water sample cannot be measured by this method. Thus artificial Al^{3+} contaminated tap water samples have been prepared by adding known amounts of standard Al^{3+} solution. The prepared samples were analysed by the same UV-visspectrometer and spectro-fluorimeter. The recovery amounts were calculated using their standard calibration curves (intensity *vs.* conc.) with the help of Lambert-Beer law. As shown in Table 3a and 3b, the Al^{3+} concentration recovered for each sample is in agreement with the spiked amount with good precision (RSD values of 0.98% and 0.43% by colorimetric and fluorometric methods, respectively). Thus the receptor **L** can be suitable to detect Al^{3+} ion quantitatively in real water samples.

Table 3a Determination of Al^{3+} ion in tap water samples by colorimetric method.

| Metal Ion	Spiked amount (µM)	Recovered amount(µM)	Recovery %	RSD % value
Al^{3+}	10	10.15	101.5	
	10	9.97	99.7	0.98
	10	10.11	101.3	

Table 3b Determination of Al^{3+} ion in tap water samples by fluorometric method.

Metal Ion	Spiked amount (µM)	Recovered amount(µM)	Recovery %	RSD % value
Al^{3+}	10	9.83	98.3	
	10	9.89	98.9	0.43
	10	9.91	99.1	

Molecular logic gate

The absorption band at 412 nm of the free receptor **L** has completely vanished, and the emission intensity at 380 nm was enhanced upon screening with Al^{3+} ion. These optical changes were fully recovered upon the addition of 1 equiv. of Na_2EDTA. Thus the presence of two chemical inputs Al^{3+} and Na_2EDTA, the observed output signal at 412 nm from the absorption intensity and 380 nm based on the fluorescence intensity change exactly mimic with an "IMPLICATION" logic gate with threshold value 0.04 and an "INHIBIT" logic gate with threshold value 8000 respectively. The constructed truth table has been summarised in Fig. 10.
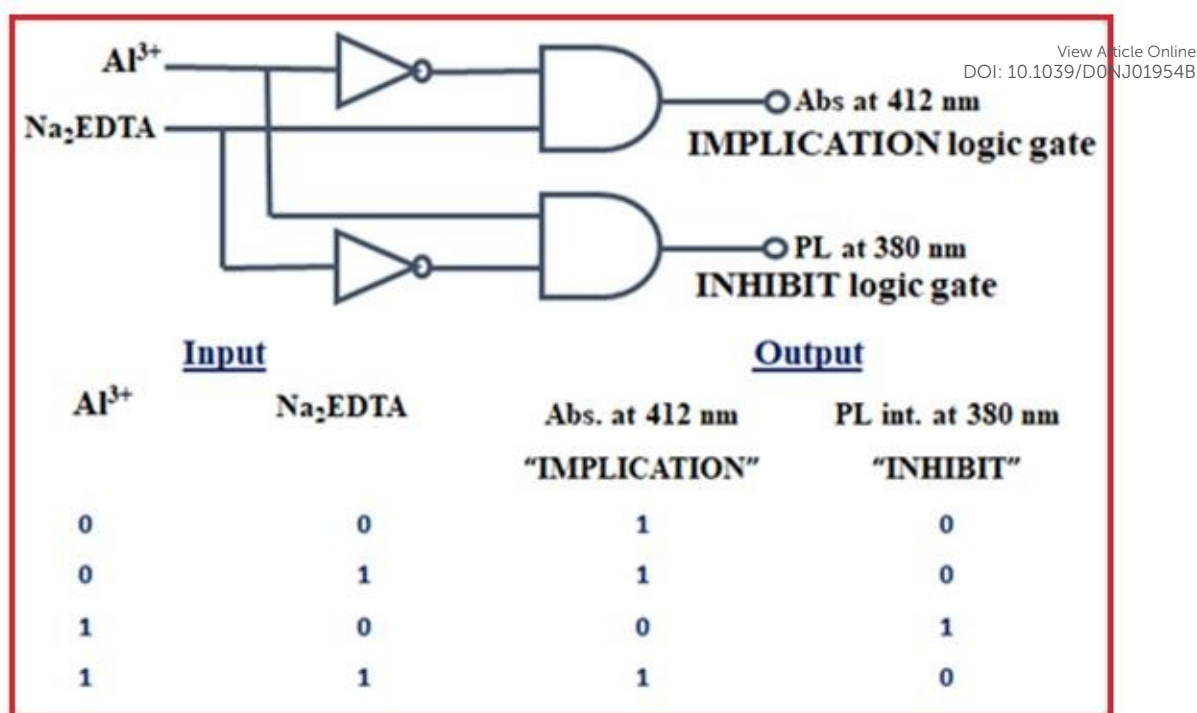
Fig. 10. Application of **L** in building molecular logic gate.

Smartphone-Based Colour Image

The colour change in the presence of Al^{3+} ions can also be applicable by easy handle able smartphone-based analysis as it produced more accurate and sensitive results than that observed visually. Here the different standard solutions of Al^{3+} ions were prepared in the tap water and added separately to the standard methanol-tris-HCl buffer (10 mM, pH 7.2) solution of receptor **L** (40μM). The representative photographs of each set of the receptor solution with different Al^{3+} ion concentration was captured by a smartphone (Fig 11a), and the three primary colour (red, green and blue) intensity values were determined (Fig 11b) by the pre-installed app RGB grabber shunamicode. The photograph capturing was carried out in a 40 w LED confined square box to reduce the external light effect and to keep the fixed distance of the solution from the smartphone. With the concentration Al^{3+} ion rising from 0 to 16, the colour of the solution shifted from yellow to colourless accompanied with the increase of its complementary colour blue much more sharply than the other two. This linear increase of blue colour value with the analyte concentration can be used to construct calibration curve (Fig 11c) and the calculated detection limit value 1.36×10^{-7} M based on the same equation 3σ/m. Within this range, any unknown Al^{3+} ion concentration (e.g. X) can be calculated by measuring its blue colour value.
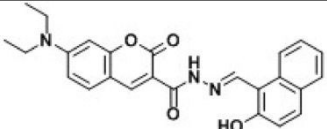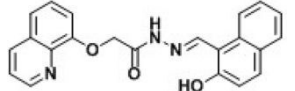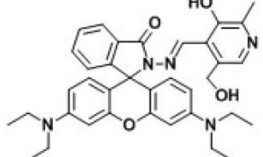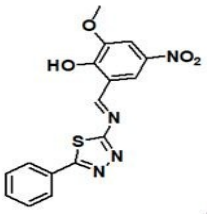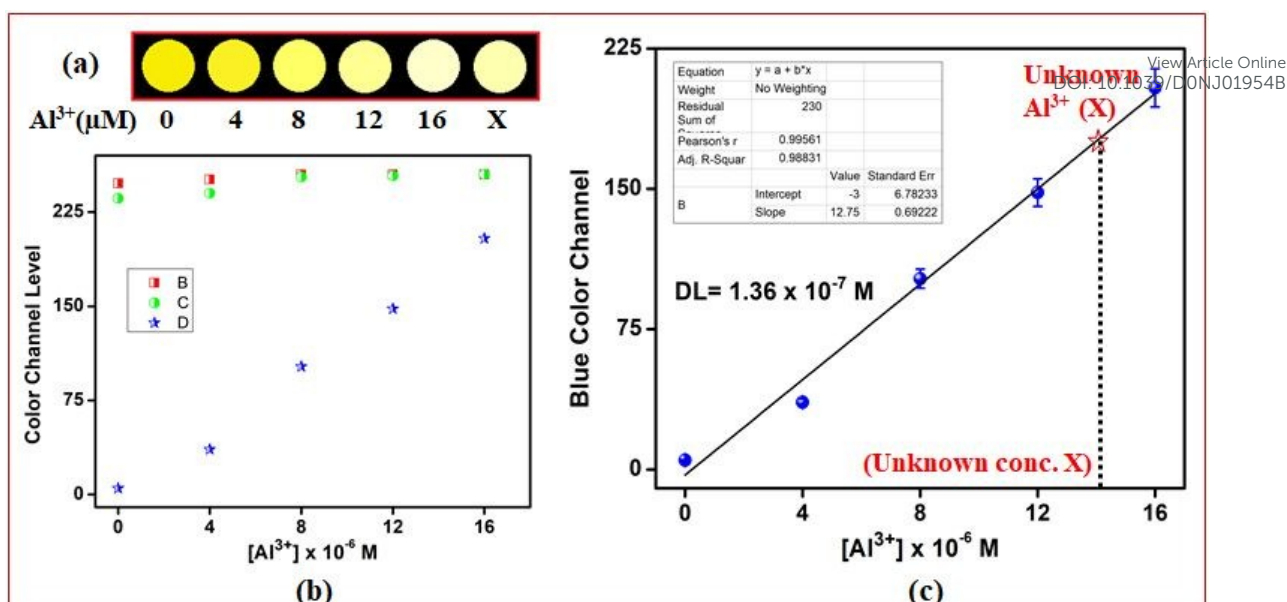
Fig. 11. (a) Smartphone-based colour image; (b) Plot of red, green and blue colour channel level of signal images obtained from the smartphone using RGB grabber shunamicode and (c) Plot of blue colour channel level.

Comparison of L with other Schiff base fluorescent, colourimetric chemosensor

The performance of the fluorescent, colourimetric sensing action of the Schiff base probe **L** towards Al^{3+} was compared with some other reported fluorescent, colourimetric Schiff base chemosensors, as listed in Table 4. It can be seen from Table 4, compared to the other systems, present system has a number of attractive analytical features, such as high sensitivity, wide linear range, high selectivity, lower detection limit, simple operation technology, good solubility, visualised sensitive and good practical applicability. Moreover, the synthesis of the proposed chemosensor **L** requires only two steps and less hazardous reagents and no hazardous by-product is formed.

Table 4. Comparison of **L** with other reported Schiff base fluorescent, colourimetric chemosensor

Probe	Solvent	LOD	Application	Ref.
	EtOH	8.2×10^{-7} M	No application reported	52
	EtOH	7.2×10^{-7} M	No application reported	53
	DMSO-H_2O (9:1, v/v)	6.0×10^{-7} M	No application reported	54
	EtOH	1.9×10^{-7} M	No application reported	55

	EtOH-H_2O (9:1, v/v)	3.3×10^{-6} M	No application reported	56
	MeCN-H_2O (1:4, v/v)	1.5×10^{-6} M	No application reported	57
	H_2O	1.9×10^{-6} M	No application reported	58
	MeOH-*tris*-HCl buffer (10 mM, pH 7.2, 1:1 v/v)	1.15×10^{-7} M	Application in real water samples, building the molecular logic gate and smartphone-based application.	This work

Conclusions

In summary, we have developed a thiadiazole based Schiff base receptor **L** in a simple way which can effectively recognise Al^{3+} with high selectivity and good sensitivity in the presence of other metal ions. The LOD of **L** towards Al^{3+} was calculated to 1.43×10^{-7} M by colourimetry and 1.15×10^{-7} M by fluorometry. When **L** exploited with Al^{3+}, the fluorescent emission peak appeared at 380 nm on excitation at 310 nm. The colour change of the solution was observed directly by the naked eye from yellow to colourless. The interaction between **L** and Al^{3+} was studied by Job's plot, ESI-MS spectrometry, DFT and TDDFT calculations. **L** can detect Al^{3+} through "*off−on−off*" type fluorescent signalling. Moreover, **L** could operate in a wide range of pH and can be successfully applied for detection and quantification of Al^{3+} in environmental samples, smartphone-based analysis and for building IMPLICATION and INHIBIT type of logic gates.

Acknowledgements

Supporting Information Summary

CCDC number 1993595 contains the supplementary crystallographic data for **1** and complex **1**. The data can be obtained free of charge from the Cambridge Crytallographic Data Centre, 12 Union Road, Cambridge CB21EZ, UK; Fax: (+44)1223-336-033; or email: deposit@ccdc.cam.ac.uk:

Supplementary data containing Fig. S1- S20 and Tables S1-S2 of this article can be found online at…………………………..

Conflicts of interest

Authors declare no conflicts of interest.

References

1. R. M.Máñez and F. Sancenón, *Chem. Rev.,* 2003, **103**, 4419−4476.

2. H. Sharma, N. Kaur, A. Singh, A. Kuwar and N. Singh, *J. Mater. Chem. C*, 2016, **4**, 5154-5194.

3. K. P. Carter, A. M. Young and A. E. Palmer, *Chem. Rev.,* 2014, **114**, 4564−4601.

4. A.Hulanicki, S. Glab and F. Ingman, *Pure Appl. Chem.*, 1991, **63**, 1247−1250.

5. P. Ghosh, K. Pramanik, S. Paul, P. Malpaharia, S. K. Chandra, S. K. Mukhopadhyay and P. Banerjee, *ACS Appl. Bio Mater.,* 2018, **1**, 683-692.

6. K. Rout, A.K. Manna, M. Sahu, J. Mondal, S.K. Singh, G.K. Patra, *RSC Advances,* 2019, **9**, 25919-25931.

7. Y. H. Zhao, X. Zeng, L. Mua, J. Li, C. Redshaw and G. Wei, *Sens. Actuators B*, 2014, 204, 450–458.

8. J. C. Qin, Z. Y. Yang and P. Yang, *Inorg. Chim. Acta*, 2015, 432, 136–141.

9. F. Yu, L. J. Hou, L. Y. Qin, J. B. Chao, Y. Wang and W. J. Jin, *J. Photochem. Photobiol., A*, 2016, 315, 8–13.

10. P. J. Hung, J. L. Chir, W. Ting and A. T. Wu, *J. Lumin.*, 2015, 158, 371–375.

11. P. Torawane, K. Tayade, S. Bothra, S. K. Sahoo, N. Singh and A. Borse, *Sens. Actuators, B*, 2016, 222, 562–566.

12. A. Gupta and N. Kumar, RSC Advances, 2016, 6, 106413-106434.

13. K.Velmurugan, S. Mathankumar, S. Santoshkumar, S. Amudha and R. Nandhakumar, *Spectrochim. Acta, A,* 2015, **139**, 119-123.

14. S. Samanta, S. Goswami, M.N. Hoque, A. Ramesh and G. Das, *Chem. Commun.*, 2014, **50**, 11833.

15. A. Ghorai, J. Mondal, R. Chandra and G.K. Patra, *Dalton Trans.*, 2015, **44**, 13261-13271.

16. G. Ciardelli and N. Ranieri, *Water Res.,* 2001, **35**, 567−572.

17. A. Ghorai, J. Mondal, S. Chowdhury and G.K. Patra, *Dalton Trans.*, 2016, **45**, 11540-11553.

18. D. Krewski, R.A. Yokel, E. Nieboer, D. Borchelt, J. Cohen, J. Harry, S. Kacew, J. Lindsay, A.M. Mahfouz and V. Rondeau, *J. Toxicol. Environ. Health, Part B*, 2007, **10**, 1−269.

19. C. Exley, *Environ. Sci. Process.,* 2013, **15**, 1807−1816.

20. S. Sinha, B. Chowdhury and P. Ghosh, *Inorg. Chem.,* 2016, **55**, 9212−9220.

21. Y.J. Liu, F.F. Tian, X.Y. Fan, F.L. Jiang and Y. Liu, *Sensors & Actuators B Chemical*, 2017, **240**, 916-925.

22. F. Wang, Y. Xu, S.O. Aderinto, H. Peng, H. Zhang and H. Wu, *Journal of Photochemistry & Photobiology A, Chemistry*, 2017, **332**, 273-282.

23. Z. Li, J. Zhao, Y. Wu, L. Mu, X. Zeng, Z. Jin, G. Wei, N. Xie and C. Redshaw, *Org. & Biomol. Chem.*, 2017, **15**, 8627-8633.

24. K. Mizutani, B. Mikami, S. Aibara, and M. Hirose, *Acta Crystallogr., Sect. D: Biol. Crystallogr*. 2005, **61**, 1636−1642.

25. J.J.R.F. da Silva and R.J.P. Williams, *OUP: Oxford, U.K.*, 2001.

26. M. Kumar and A. Puri, *Indian J.Occup Environ. Med.* 2012, **16**, 40–44.

27. R. Michalski, 2009, **39**, 230–250,

28. S. L. C. Ferreira, A. S. Queiroz, M. S. Fernandes and H. C. dos Santos, *Spectrochim. Acta B,* 2002, **57**, 1939-1950.

29. D. Shan, C. Mousty and S. Cosnier, *Anal. Chem.,* 2004, **76**, 178-183.

30. M. H. Mashhadizadeh, M. Pesteh, M. Talakesh, I. Sheikhshoaie, M. M. Ardakani and M.A. Karimi, *Spectrochim. Acta B*, 2008, **63**, 885-888.

31. H. J. Jang, J. H. Kang, D. Yun and C. Kim, *Photochem. Photobiol. Sci.*, 2018, **17**, 1247-1255.

32. G.K. Patra, R. Chandra, A. Ghorai and K. K. Shrivas, *Inorg. Chim. Acta*, 2017, **462**, 315-322.

33. A. Ghorai, J. Mondal, R. Saha, S. Bhattacharya, G.K. Patra, *Anal. Methods*, 2016, **8**, 2032-2040.

34. A. Ghorai, J. Mondal and G.K. Patra, New J. Chem., 2016, **40**, 7821-7830

35. A. K Manna, K. Rout, S. Chowdhury and G. K. Patra, *Photochem.&Photobiol. Sciences*, 2019, **18**, 1512-1525.

36. *SMART& SAINT Software Reference manuals*, version 5.0; Bruker AXS Inc.: Madison,WI, 1998.

37. T. Gruene, H. W. Hahn, A. V. Luebben, F. Meilleur and G. M. Sheldrick, *J. Appl. Cryst*., 2014, **47**, 462-466.

38. (a) L.J. Farrugia, WinGX: an integrated system of windows programs for the solution, refinement and analysis for single crystal x-ray diffraction data, version 1.80.01; Department of Chemistry: University of Glasgow, 2003; (b) L.J. Farrugia, *J. Appl. Crystallogr.*, 1999, **32**, 837-838.

39. K. R. Kumar, B. L. Rani and K.N.S. Karthik, *Am. J. Pharm. Tech. Res.,* 2017, **7**, 1-4.

40. M.J. Frisch, G.W. Trucks, H.B. Schlegel, G.E. Scuseria, M.A. Robb, J.R. Cheeseman, G. Scalmani, V. Barone, B. Mennucci, G.A. Petersson, H. Nakatsuji, M. Caricato, X. Li, H.P.

Hratchian, A.F. Izmaylov, J. Bloino, G. Zheng, J.L. Sonnenberg, M. Hada, M. Ehara, K. Toyota, R. Fukuda, J. Hasegawa, M. Ishida, T. Nakajima, Y. Honda, O. Kitao, H. Nakai, T. Vreven, J.A. Montgomery, Jr., J.E. Peralta, F. Ogliaro, M. Bearpark, J.J. Heyd, E. Brothers, K.N. Kudin, V.N. Staroverov, R. Kobayashi, J. Normand, K. Raghavachari, A. Rendell, J.C. Burant, S.S. Iyengar, J. Tomasi, M. Cossi, N. Rega, J.M. Millam, M. Klene, J.E. Knox, J.B. Cross, V. Bakken, C. Adamo, J. Jaramillo, R. Gomperts, R.E. Stratmann, O. Yazyev, A.J. Austin, R. Cammi, C. Pomelli, J.W. Ochterski, R.L. Martin, K. Morokuma, V.G. Zakrzewski, G.A. Voth, P. Salvador, J.J. Dannenberg, S. Dapprich, A.D. Daniels, Ö. Farkas, J.B. Foresman, J.V. Ortiz, J. Cioslowski, D.J. Fox, Gaussian 09, Revision C.01, Gaussian Inc., Wallingford, CT 2009.

41. A.D. Becke, *J. Chem. Phys.*, 1993, **98**, 5648-5652.

42. (a) P.J. Hay and W.R. Wadt, *J. Chem. Phys.*, 1985, **82**, 299-310; (b) P.J. Hay and W.R. Wadt., *J. Chem. Phys.*, 1985, **82**, 270-283.

43. V. Barone and M. Cossi., *J. Phys. Chem. A*, 1998, **102**, 1995-2001.

44. J. Tomasi, B. Mennucci and R. Cammi, *Chem. Rev.*, 2005, **105**, 2999-3094.

45. D. Qi, X. Chen and J. Jiang, *Comp. & Theo. Chem.*, 2020, **1181**, 112832.

46. H. Zhu, M. Li, J. Hu, X. Wang, J. Jie, Q. Guo, C. Chen and A. Xia, *Scientific Reports*, 2016, **6**, 24313-24320.

47. L.-Q. Yan, M.-F. Cui, Y. Zhou, Y. Ma, and Z. Jian, *Anal. Sciences*, 2015, **31**, 1055-1059.

48. (a) T. W. Myers, N. Kazem, S. Stoll, R. D. Britt, M. Shanmugam and L. A. Berben, *J. Am. Chem. Soc.,* 2011, **133**, 8662−8672; (b) R. Mondol and E. Otten, *Inorg. Chem.*, 2019, **58**, 6344-6355.

49. (a) D. Simond, S. E. Clifford, A. F. Vieira, C. Besnard and A. F. Williams, *RSC Adv.*, 2014, **4**, 16686-16693; (b) D. Lundberg and K. Lyczko, *Acta Cryst.*, 2015, **71**, 895–898.

50. L. C. Liang, F. Y. Chen, M. H. Huang, L. C. Cheng, C. W. Li and H. M. Lee, *Dalton Trans.*, 2010, **39**, 9941–9951.

51. S. Chowdhury, A. Bhattacharya, P. Saha, S. Majumder, E. Suresh and J. P. Naskar, *J. Coord. Chem.*, 2016, **69**, 3664-3676.

52. J.C. Qin, T.R. Li, B.D. Wang ,Z.Y. Yang and L. Fan, *Spectrochim. Acta A,* 2014, **133**, 38-43.

53. J.C. Qin, Z.Y. Yang, L. Fan, X.Y. Cheng, T.R. Li and B.D. Wang, *Anal. Methods*, 2014, **6**, 7343-7348

54. Z. Kejík, R. Kaplánek, M. Havlík, T. Bříza, D. Vavřinová,B, Dolenský, P. Martásek and V. Král, *J. Luminescence,* 2016, **180**, 269–277.

55. L. Fan, T.R. Li, B.D. Wang, Z.Y. Yang, C.J. Liu and L. Fan, *Spectrochim. Acta A*, 2014, **118**, 760-764.

56. J. C. Qin and Z.Y. Yang, *Anal. Methods*, 2015, **7**, 2036-2040.

57. C.R. Li, Z.C. Liao, J.C. Qin, B.D. Wang and Z.Y. Yang, *J. Lumin.*, 2015, **168**, 330-333.

58. Q. Huang, Q. Zhang, E. Wang, Y. Zhou, H. Qiao, L. Pang and F. Yu, *Spectrochim. Acta A,* 2016, **152**, 70-76.

GRAPHICAL ABSTRACT

Combined experimental and theoretical studies on Phenyl thiadiazole based novel turn-on fluorescent colorimetric Schiff base chemosensor for the selective and sensitive detection of Al³⁺

Amit Kumar Manna,[a] Shubhamoy Chowdhury[b] and Goutam K. Patra[a]*

[a]Department of Chemistry, Guru Ghasidas Vishwavidyalaya, Bilaspur (C.G), India

[b]Department of Chemistry, Gour Banga University, Malda, West Bengal   732 103, India

Phenyl thiadiazole based Schiff base receptor (**L**) has been presented for the first time for turn-on fluorescent colorimetric detection of Al³⁺ ion. The chemosensor **L** displayed very quick response, excellent selectivity and sensitivity towards Al³⁺ ion, both by colourimetry and fluorometry with very low detection limit in aqueous medium. The binding stoichiometry was obtained as 2:1 from job's plot analysis, ESI-MS spectra and DFT and TDDFT studies. The chemosensor **L** can be applied for the formation of binary logical devices, recovery of contaminated water samples and smart-phone based chemical analysis.